Available online at www.sciencedirect.com
SCIENCE DIRECT®
Journal of Power Sources 122 (2003) 9–18
JOURNAL OF POWER SOURCES
www.elsevier.com/locate/jpowsour

Performance comparison of Fick's, dusty-gas and Stefan–Maxwell models to predict the concentration overpotential of a SOFC anode

R. Suwanwarangkul [a], E. Croiset [a,*], M.W. Fowler [a], P.L. Douglas [a], E. Entchev [b], M.A. Douglas [b]

[a] *Department of Chemical Engineering, 200 University Ave. West, University of Waterloo, Waterloo, ON, Canada N2L 3G1*
[b] *Advanced Combustion Technologies Laboratory, CANMET Energy Technology Centre, 1 Haanel Drive, Ottawa, ON, Canada K1A 1M1*

Received 23 November 2002; accepted 1 December 2002

Abstract

Models for mass transport inside a porous SOFC anode were developed based on Fick's model (FM), the dusty-gas model (DGM) and the Stefan–Maxwell model (SMM) to predict the concentration overpotential. All models were validated with experimental data for H_2–H_2O–Ar and CO–CO_2 systems. The effect of pore size on all model predictions was discussed. It was concluded that the dusty-gas model is the most appropriate model to simulate gas transport phenomena inside a SOFC anode. However, this model requires numerical solution, whereas Fick's and Stefan–Maxwell's do not. It was found that the SMM, rather than the FM, is a good approximation of the dusty-gas model for H_2–H_2O system, except in the case of high current density, low H_2 concentration and low porosity, where only the DGM is recommended. For the CO–CO_2 system, there is no simple rule for selecting an alternate model to DGM. Depending on the CO concentration, porosity and current density, the FM or the SMM could be used. The only restriction is for small porosities where only the DGM should be used. This paper also demonstrated that only the DGM is recommended for a multicomponent system (H_2–H_2O–CO–CO_2).

Keywords: SOFC; Mass transport model; Fick's model; Dusty-gas model; Stefan–Maxwell model; Concentration overpotential

1. Introduction

Solid oxide fuel cells (SOFCs) promise electricity generating processes for stationary applications in the mid-term future. This is because the electrical efficiency typically achieved in a SOFC is much greater than that obtained from a conventional heat engine and any other type of fuel cells [1]. Furthermore, additional efficiency can be gained by adding a bottoming cycle to recover heat from hot gas exhausted from a SOFC. Another key advantage is that a SOFC can operate with CO, which is a poison in other types of fuel cells. Nowadays, three basic designs are studied; they are cathode-, electrolyte- and anode-supported designs. The latter design has been considered to be better than any other designs because it can operate at lower temperature and the highest performance can be achieved [2–4].

It has been reported [3,4] that the performance of an anode-supported SOFC at high operating current density or high fuel utilization is governed by the concentration overpotential at the anode side. This can be explained by the fact that, at high demands, the requirement for the reactant exceeds its capability to diffuse through the relatively thick porous ceramic anode to the reaction site at the vicinity of the anode–electrolyte interface [5]. For this reason, the accurate prediction of the anodic concentration overpotential is extremely important. In particular, for a tubular anode-supported SOFC where high fuel utilization is required, a small error in the concentration overpotential calculation may cause a dramatic change to its design performance.

The anodic concentration overpotential considers the difference in gas concentrations between the anode–electrolyte interface and the bulk. Mass transport models inside the porous SOFC anode must be applied to estimate gas concentrations at the anode–electrolyte interface. However, such a mass transport model needs to be sophisticated enough so that it can take into account parameters such as complex functions of temperature, pressure, gas concentrations, and the physical properties of SOFC materials like porosity, tortuosity and pore size of the electrode materials.

The transport of gaseous components through porous media has been extensively studied over the years as described

* Corresponding author. Tel.: +1-519-888-4567x6472; fax: +1-519-746-4979.
E-mail address: ecroiset@uwaterloo.ca (E. Croiset).

0378-7753/03/$ – see front matter
doi:10.1016/S0378-7753(02)00724-3

Nomenclature

B_o	pore characteristics
D_i^{eff}	overall effective diffusion coefficient of component i (cm^2/s)
D_{im}^{eff}	molecular diffusion coefficient of component i in all other components present in the mixture (cm^2/s)
$D_{i,k}^{eff}$	knudsen diffusion coefficient of component i (cm^2/s)
DGM	dusty-gas model
F	Faraday's constant (96500 C/mol)
FM	Fick's model
J	operating current density (A/cm^2)
M_i	molecular weight of component i
N_i	mol flux of gas species i ($mol/(cm^2\,s)$)
P	operating pressure (atm)
R	gas constant (8.31441 J/(mol K))
r_i	rate of reaction inside porous media ($mol/(m^3\,s)$)
SMM	Stefan–Maxwell model
T	operating temperature (K)
y_i	mole fraction of component i

Greek letters

α	parameter defined by Eq. (18)
ε	porosity (fraction)
η_{Conc}	concentration overpotential (mV)
μ	viscosity (N/ms)
τ	tortuosity

Subscripts and superscripts

A/E	interface between anode and electrolyte
B	binary component system
T	ternary component system

in many references [6–8]. In general, mass transport of components inside porous media can be described using either the extended Fick's model (FM) or the dusty-gas model (DGM) as explained in [8]. Both FM and the DGM are mass transport equations taking into account Knudsen diffusion, molecular diffusion and the effect of a finite pressure gradient. The key feature of the DGM differs from that of FM in that the flux ratio in DGM depends on the square-root of gas molecular weight. From a literature review, although the DGM is superior to FM in its capability to predict the fluxes inside porous media [9], FM is more frequently used because it allows explicit analytical expressions to be derived for fluxes. Furthermore, Veldsink et al. [10] claimed that the deviation between FM and the DGM can be neglected for the description of transport and reactions in a porous catalyst. In SOFC modelling, numerous studies on gas transport phenomena [2,4,11,12] have been carried out using FM. Some other references [13,14] eliminated out the effect of Knudsen diffusion leaving on by the Stefan–Maxwell model in their mass transport equations. Only Yakabe et al. [3] and Lehnert et al. [5] used more complex mass transport models, which were similar to the DGM. However, their mass transport models were complex and required numerical methods to obtain the solution. Consequently, the objective of this paper is to evaluate the various mass transport models by validating them with the measured concentration overpotential data obtained from Yakabe et al. [3]. The binary systems of H_2–H_2O and CO–CO_2 as well as the ternary systems of H_2–H_2O–Ar are considered.

2. Model development

2.1. Modelling assumptions

The modelling assumptions are consistent with those used by Yakabe et al. [3], and they are as follows:

1. H_2 and CO are the anodic reactants. Only binary gas mixtures of CO–CO_2 and H_2–H_2O and a ternary gas mixture of H_2–H_2O–Ar are considered.
2. Gas concentrations are uniform along the fuel channel. This assumption is valid because the length of the fuel channel is very small (20 mm). Fuel utilization is less than 5% and, therefore, assumed to be constant. Accordingly, only a 1D model in the z-direction was examined as shown in Fig. 1.
3. The current density is uniform over the entire electrodes. This assumption is valid as long as the gas concentration is assumed to be uniform along the fuel channel, because the current density produced is related to the amount of reactant gas diffusing into the anode layer.
4. Steady-state condition.

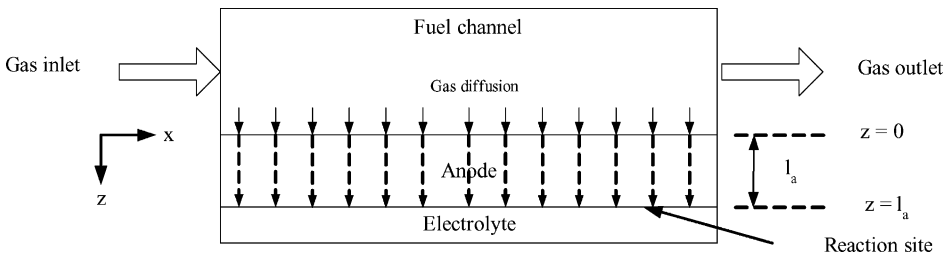

Fig. 1. A SOFC geometry used in model development. The model is focused on diffusion inside a porous anode layer.

5. Temperature and total pressure are constant throughout the entire electrode. The total pressure gradient inside the electrode is assumed to be negligible. This assumption is quite reasonable since there is no net change in the number of moles in the gas phase [8] due to electrochemical reactions. Consider the electrochemical reactions of H_2 and CO at the anode:

$$H_2 + O^{2-} \rightarrow H_2O + 2e^- \quad \text{(a)}$$

$$CO + O^{2-} \rightarrow CO_2 + 2e^- \quad \text{(b)}$$

6. From reactions (a) and (b), it is found that there is no net change in the number of moles in the gas phase.
7. Finally, Lehnert et al. [5] reported that the electrochemical conversion occurs in the vicinity of the electrolyte–anode interface. The depth of the reaction zone is about 50 μm above the anode–electrolyte interface. This is very small compared to the 2 mm anode thickness in the SOFC from Yakabe et al. [3]. Therefore, it can be assumed that the electrochemical reaction is a heterogeneous reaction, which takes place at the anode–electrolyte interface.

2.2. Mass transport equations

Mass transport through porous medium can be determined using concepts described in [8,10]. For a single component, the mass transport equation can be written as

$$\frac{\varepsilon}{RT}\frac{\partial(y_i P)}{\partial t} = -\nabla \cdot N_i + r_i \ (\text{mol m}^{-3}\,\text{s}^{-1}) \quad (1)$$

where ε and N_i represent the porosity and the rate of mass transport, respectively, into porous media. r_i is the rate of reaction inside the porous medium. The term on the left-hand side is valid when unsteady state is approached. The first and second terms on the right-hand side represent the diffusion rate and the rate of reaction inside the porous medium. It was assumed earlier that the diffusion process is at steady state and that the electrochemical reactions take place at the boundary of the anode–electrolyte interface rather than throughout the porous medium. Therefore, within the anode, only the first term on the right-hand side is significant, Eq. (1), therefore, becomes

$$\nabla \cdot N_i = 0 \quad (2)$$

The rate of mass transport, N_i, generally depends on the operating conditions (reactant concentration, temperature and pressure) and the microstructure of material (porosity, tortuosity and pore size). Three models were used to develop expressions for N_i: Fick's, the dusty-gas and the Stefan–Maxwell models.

2.2.1. Fick's model

FM is the simplest form used to describe the transport of components through the gas phase and within porous media. The general extended form of this model [10] takes into account diffusion and convection transport and is given by:

$$N_i = \frac{1}{RT}\left(-D_i^{\text{eff}}\frac{\partial(y_i P)}{\partial z} + \frac{B_o y_i P}{\mu}\frac{\partial P}{\partial z}\right) \quad (i = 1, \ldots, n) \quad (3)$$

where B_o is the permeability coefficient, D_i^{eff} the effective diffusivity of species i, and μ the viscosity of the gas. The first and second terms on the right-hand side account for diffusion and convection transport, respectively. It is noted that the convection transport term is described by the Darcy equation. However, it is assumed that the total pressure change within the pore is insignificant ($\text{d}P/\text{d}z \approx 0$). Thus, only the diffusion transport is necessary to determine the rate of mass transport Eq. (3) reduces to:

$$N_i = \frac{-D_i^{\text{eff}}}{RT}\frac{\partial(y_i P)}{\partial z} \quad (i = 1, \ldots, n) \quad (4)$$

The diffusion process within a pore can be typically divided into two diffusion mechanisms: molecular diffusion and Knudsen diffusion. Molecular diffusion is dominant for large pore sizes and high system pressures while Knudsen diffusion becomes significant when the mean-free path of the molecular species is much larger than the pore size. Therefore, D_i^{eff} can be written by combining the effective molecular diffusion (D_{im}^{eff}) and effective Knudsen diffusion ($D_{i,k}^{\text{eff}}$) coefficients as follows (Bosanquet formula) [10]:

$$D_i^{\text{eff}} = \left(\frac{1}{D_{im}^{\text{eff}}} + \frac{1}{D_{i,k}^{\text{eff}}}\right)^{-1} \quad (5)$$

D_{im}^{eff} and $D_{i,k}^{\text{eff}}$ depend on the microstructure of the porous anode (porosity, particle size and tortuosity) and on the operating conditions (temperature and pressure). The calculation of these parameters are described in [3,4]. It is noted that D_i^{eff} given in Eq. (5) is derived from the assumption of equimolar counter diffusion of reactant and product species.

For binary component systems (H_2(1)–H_2O(2) and CO(1)–CO_2(2)), Eq. (4) becomes

$$N_1 = -\frac{D_{1,\text{B}}^{\text{eff}} P}{RT}\frac{\text{d}y_1}{\text{d}z} \quad (6)$$

where $D_{1,\text{B}}^{\text{eff}}$ represents the effective diffusion for binary systems as follows:

$$D_{1,\text{B}}^{\text{eff}} = \left(\frac{1}{D_{12}^{\text{eff}}} + \frac{1}{D_{1,k}^{\text{eff}}}\right)^{-1} \quad (7)$$

At the anode–electrolyte interface ($z = l_a$, see Fig. 1), the amount of current density produced is governed by the rate of reactant diffusing into the porous anode, i.e. $N_1 = -J/2F$, where J is the operating current density and F the Faraday's constant. Therefore,

$$\left.\frac{\text{d}y_1}{\text{d}z}\right|_{z=l_a} = -\frac{JRT}{2FD_{1,\text{B}}^{\text{eff}} P} \quad (8)$$

Inserting Eq. (6) into Eq. (2) and solving yields to the following mole fraction profile:

$$y_1 = C_1 + C_2 z \tag{9}$$

where C_1 and C_2 are constants. By using the Neuman boundary condition at $z = l_a$ (Eq. (8)) and the Dirichlet boundary condition $y_i|_{z=0} = y_{i,\text{bulk}}$, C_1 and C_2 are determined and Eq. (9) becomes:

$$y_1 = y_{1,\text{bulk}} - \frac{JRT}{2FD^{\text{eff}}_{1,\text{B}}P} z \tag{10}$$

y_2 can be determined by the fact that $y_1 + y_2 = 1$.

For ternary component systems (H_2(1)–H_2O(2)–Ar), the formula used to calculate y_1 and y_2 are similar to the one indicated in Eq. (10) except that the overall effective diffusion coefficient for the ternary component system ($D^{\text{eff}}_{1,\text{T}}$) is derived from the Stefan–Maxwell relation. The mole fraction of component 1 inside the porous anode is expressed as follows:

$$y_1 = y_{1,\text{bulk}} - \frac{JRT}{2FD^{\text{eff}}_{1,\text{T}}P} z \tag{11}$$

where

$$D^{\text{eff}}_{1,\text{T}} = \frac{1}{(1/D^{\text{eff}}_{1,k}) + (1/D^{\text{eff}}_{1\,\text{Ar}}) + ((1/D^{\text{eff}}_{12}) - (1/D^{\text{eff}}_{1\,\text{Ar}}))(1 - y_{\text{Ar}})} \tag{12}$$

and, where $D^{\text{eff}}_{1\,\text{Ar}}$ is the effective binary diffusion coefficient of component 1 in argon, y_{Ar} represents the mole fraction of argon present in the gaseous mixtures.

2.2.2. Dusty-gas model (DGM)

The DGM includes the Stefan–Maxwell formulation and takes into account Knudsen diffusion [15]. It is assumed from this model that pore walls consist of giant molecules ('dust') uniformly distributed in space. These dust molecules are considered to be a dummy, or pseudo, species in the mixture. The general form of the DGM is shown in Eq. (13):

$$\frac{N_i}{D^{\text{eff}}_{i,k}} + \sum_{j=1, j\neq i}^{n} \frac{y_j N_i - y_i N_j}{D^{\text{eff}}_{ij}} = -\frac{1}{RT}\left(P\frac{\mathrm{d}y_i}{\mathrm{d}z} + y_i \frac{\mathrm{d}P}{\mathrm{d}z}\left(1 + \frac{B_0 P}{D^{\text{eff}}_{i,k}\mu}\right)\right) \tag{13}$$

The second term on the right-hand side is called the permeation flux and is applied to take into account the effect of total pressure gradient on mass transport. However, it is assumed in this study that the total pressure is uniform over the entire depth of the porous anode. Thus, the definite total pressure gradient term can be ignored. Consequently, only the diffusion flux is addressed. Eq. (13) reduces to:

$$\frac{N_i}{D^{\text{eff}}_{i,k}} + \sum_{j=1, j\neq i}^{n} \frac{y_j N_i - y_i N_j}{D^{\text{eff}}_{ij}} = -\frac{P}{RT}\frac{\mathrm{d}y_i}{\mathrm{d}z} \tag{14}$$

For diffusion with heterogeneous chemical reaction, the flux ratios are governed by reaction stoichiometry. Summing Eq. (14) over the n species leads to the Graham's law of diffusion in gaseous mixtures [8].

$$\sum_{i=1}^{n} N_i \sqrt{M_i} = 0 \tag{15}$$

where M_i is the molecular weight of component i.

For two binary component systems (H_2(1)–H_2O(2) and CO(1)–CO_2(2)), Eq. (14) becomes

$$\frac{N_1}{D^{\text{eff}}_{1,k}} + \frac{y_2 N_1 - y_1 N_2}{D^{\text{eff}}_{12}} = -\frac{P}{RT}\frac{\mathrm{d}y_1}{\mathrm{d}z} \tag{16}$$

Rearranging Eq. (16) gives,

$$N_1\left(\frac{1}{D^{\text{eff}}_{1,k}} + \frac{y_2 - y_1 N_2/N_1}{D^{\text{eff}}_{12}}\right) = -\frac{P}{RT}\frac{\mathrm{d}y_1}{\mathrm{d}z} \tag{17}$$

Because $y_2 = 1 - y_1$ and $N_2/N_1 = -\sqrt{M_1/M_2}$ (Graham's law), N_1 can be written as follow:

$$N_1 = -\frac{P}{RT}\left[\frac{1 - \alpha y_1}{D^{\text{eff}}_{12}} + \frac{1}{D^{\text{eff}}_{1,k}}\right]^{-1}\frac{\mathrm{d}y_1}{\mathrm{d}z} \tag{18}$$

where

$$\alpha = 1 - \left(\frac{M_1}{M_2}\right)^{1/2}$$

Substituting Eq. (18) into Eq. (2) gives

$$\frac{\mathrm{d}^2 y_1}{\mathrm{d}z^2} + \frac{\alpha}{D^{\text{eff}}_{12}}\left[\frac{1 - \alpha y_1}{D^{\text{eff}}_{12}} + \frac{1}{D^{\text{eff}}_{1,k}}\right]^{-1}\left(\frac{\mathrm{d}y_1}{\mathrm{d}z}\right)^2 = 0 \tag{19}$$

Eq. (19) is in the form of an ordinary differential equation, which can be solved by using the two following initial conditions:

$$\text{IC.1}: \quad y_1|_{z=0} = y_{1,\text{bulk}}$$

$$\text{IC.2}: \quad \left.\frac{\mathrm{d}y_1}{\mathrm{d}z}\right|_{z=0} = -\frac{JRT}{2PF}\left[\frac{1 - \alpha y_{1,\text{bulk}}}{D^{\text{eff}}_{12}} + \frac{1}{D^{\text{eff}}_{1,k}}\right]$$

Similarly, for ternary component systems (H_2(1)–H_2O(2)–Ar), the differential equation for component i derived from Eq. (16) is as follows

$$\frac{\mathrm{d}^2 y_1}{\mathrm{d}z^2} + \frac{\alpha}{D^{\text{eff}}_{12}}\left[\frac{1}{D^{\text{eff}}_{1,k}} + \frac{1}{D^{\text{eff}}_{1\,\text{Ar}}} + (1 - y_{\text{Ar}})\left(\frac{1}{D^{\text{eff}}_{12}} - \frac{1}{D^{\text{eff}}_{1\,\text{Ar}}}\right) - \frac{\alpha y_1}{D^{\text{eff}}_{12}}\right]^{-1}\left(\frac{\mathrm{d}y_1}{\mathrm{d}z}\right)^2 = 0 \tag{20}$$

The two initial conditions are:

$$\text{IC.1}: \quad y_i|_{z=0} = y_{i,\text{bulk}}$$

$$\text{IC.2}: \quad \left.\frac{\mathrm{d}y_i}{\mathrm{d}z}\right|_{z=0} = -\frac{JRT}{2PF}\left[\frac{1}{D^{\text{eff}}_{1,k}}+\frac{1}{D^{\text{eff}}_{1\,\text{Ar}}}+(1-y_{\text{Ar}})\left(\frac{1}{D^{\text{eff}}_{12}}-\frac{1}{D^{\text{eff}}_{1\,\text{Ar}}}\right)-\frac{\alpha y_1}{D^{\text{eff}}_{12}}\right]$$

It is difficult to find analytical expressions for Eqs. (19) and (20). Therefore, the differential equations were solved numerically in MATLAB® [16] using the provided Runge–Kutta method (*ode45*).

2.2.3. Stefan–Maxwell model (SMM)

The SMM is a well-known mass transport model applied to nonporous medium. When the Knudsen diffusion term is neglected, only the Stefan–Maxwell diffusion term is effective. Then, Eq. (14) simplifies to:

$$\sum_{j=1,\,j\neq i}^{n}\frac{y_jN_i-y_iN_j}{D^{\text{eff}}_{ij}} = -\frac{P}{RT}\frac{\mathrm{d}y_i}{\mathrm{d}x} \tag{21}$$

Eq. (21) can be solved easily using the same concept as described previously for FM. In this case, analytical solutions for binary and ternary component systems can be obtained:

$$y_1 = y_{1,\text{bulk}} - \frac{JRT}{2FD^{\text{eff}}_{12}P}z \quad \text{(binary component system)} \tag{22}$$

$$y_1 = y_{1,\text{bulk}} - \frac{JRT(D^{\text{eff}}_{1\,\text{Ar}}(1-y_{\text{Ar}})+D^{\text{eff}}_{12}y_{\text{Ar}})}{2FPD^{\text{eff}}_{12}D^{\text{eff}}_{1\,\text{Ar}}}z \quad \text{(ternary component system)} \tag{23}$$

2.3. Calculation of the concentration overpotential

The concentration overpotential used to validate the performance of various mass transport models is the difference between ideal and real cell voltage (when corrected for Ohmic and activation overpotentials). Using the Nernst potential and mole fractions of each component at the interfaces between anode and electrolyte, and mole fraction of each component in the bulk, the concentration overpotential is defined as:

$$\eta_{\text{Conc}} = -\frac{RT}{2F}\ln\left[\frac{y_{1,A/E}y_{2,\text{bulk}}}{y_{1,\text{bulk}}y_{2,A/E}}\right] \tag{24}$$

where $y_{1,A/E}$ and $y_{2,A/E}$ are mole fractions of components 1 and 2 at the interface between anode and electrolyte, respectively. The concentration overpotential for binary and ternary components for each model is calculated by inserting the mole fractions of components 1 and 2 at $z = l_a$ resulting from each model into Eq. (24).

2.3.1. Fick's model

The concentration overpotential for FM can be addressed by inserting Eq. (10) for the binary component system and Eq. (11) for the ternary component system at $z = l_a$ into Eq. (24):

$$\eta^{\text{FM}}_{\text{Conc,B}} = -\frac{RT}{2F}\ln\left[\frac{(y_{1,\text{bulk}}-(JRT/2FD^{\text{eff}}_{1,\text{B}}P)l_a)(1-y_{1,\text{bulk}})}{y_{1,\text{bulk}}(1+(JRT/2FD^{\text{eff}}_{1,\text{B}}P)l_a-y_{1,\text{bulk}})}\right] \tag{25}$$

$$\eta^{\text{FM}}_{\text{Conc,T}} = -\frac{RT}{2F} \times \ln\left[\frac{(y_{1,\text{bulk}}-(JRT/2FD^{\text{eff}}_{1,\text{T}}P)l_a)(1-y_{1,\text{bulk}}-y_{\text{Ar,bulk}})}{y_{1,\text{bulk}}(1+(JRT/2FD^{\text{eff}}_{1,\text{T}}P)l_a-y_{1,\text{bulk}}-y_{\text{Ar,bulk}})}\right] \tag{26}$$

where $D^{\text{eff}}_{1,\text{B}}$ and $D^{\text{eff}}_{1,\text{T}}$ are the overall effective diffusion coefficients for binary and ternary components, respectively, as defined by Eqs. (7) and (12).

2.3.2. Dusty-gas model

For the dusty-gas model, Eq. (19) for the binary component system and Eq. (20) for the ternary component system were solved numerically using the Runge–Kutta method to obtain the gas compositions at the reaction site. Afterwards, the calculated gas compositions were inserted into Eq. (24) to calculate the concentration overpotential.

2.3.3. Stefan–Maxwell model

The concentration overpotential when only the Stefan–Maxwell diffusion term is considered is determined by substituting Eqs. (22) and (23) into Eq. (24). The results are as follows:

$$\eta^{\text{SMM}}_{\text{Conc,B}} = -\frac{RT}{2F}\ln\left[\frac{(y_{1,\text{bulk}}-(JRT/2FD^{\text{eff}}_{12}P)l_a)(1-y_{1,\text{bulk}})}{y_{1,\text{bulk}}(1+(JRT/2FD^{\text{eff}}_{12}P)l_a-y_{1,\text{bulk}})}\right] \tag{27}$$

$$\eta^{\text{SMM}}_{\text{Conc,T}} = -\frac{RT}{2F}\ln\left[\frac{(y_{1,\text{bulk}}-(JRT(D^{\text{eff}}_{1\,\text{Ar}}(1-y_{\text{Ar}})+D^{\text{eff}}_{12}y_{\text{Ar}})/2FPD^{\text{eff}}_{12}D^{\text{eff}}_{1\,\text{Ar}})l_a)(1-y_{1,\text{bulk}}-y_{\text{Ar,bulk}})}{y_{1,\text{bulk}}(1+(JRT(D^{\text{eff}}_{1\,\text{Ar}}(1-y_{\text{Ar}})+D^{\text{eff}}_{12}y_{\text{Ar}})/2FPD^{\text{eff}}_{12}D^{\text{eff}}_{1\,\text{Ar}})l_a-y_{1,\text{bulk}}-y_{\text{Ar,bulk}})}\right] \tag{28}$$

3. Results and discussion

3.1. Model validation

All input parameters used in this model calculation were extracted from the experimental data of Yakabe et al. [3] as listed in Table 1.

The concentration overpotentials obtained from FM, the DGM and the SMM are compared with Yakabe's experimental data as illustrated in Figs. 2 and 3. These figures represent experimental data and calculated concentration overpotential for the H_2–H_2O–Ar and CO–CO_2 systems,

Table 1
Input parameters

Parameter	Symbol	Value
Operating temperature (°C)	T	750
Operating pressure(atm)	P	1
Current density (A/cm^2)	J	0.30, 0.70, 1.0 for H_2–H_2O–Ar system 0.10, 0.30, 0.50 for CO–CO_2 system
Porosity (fraction)	ε	0.46
Average pore size (μm)	$\bar{d}$	2.6
Tortuosity	τ	4.5 (fitted to experimental data)
Anode thickness (mm)	l_a	2

respectively. The aim of this experiment is to investigate the effect of reactant concentration on the concentration overpotential. The vertical axis represents the concentration overpotential (η_{Conc}) minus its basis concentration overpotential (η_{Conc0}). The horizontal axis is the reactant concentration. According to Yakabe et al. [3], η_{Conc0} is measured at $H_2/(H_2 + H_2O + Ar) = 0.8$ for H_2–H_2O–Ar and at $CO/(CO + CO_2) = 0.64$ for CO–CO_2 system. For H_2–H_2O–Ar system, a ratio of H_2:H_2O is kept at 4:1 and the concentration of H_2 in the system is varied by the degree of dilution of Argon. This means that η_{Conc0} is measured when no argon is present in the system. In this simulation, the tortuosity factor is treated as a variable parameter necessary to fit the experimental results. The results from H_2–H_2O–Ar system as illustrated in Fig. 2 are used to identify the tortuosity factor. The best fitted tortuosity factor is about 4.5, which is in the range of reported value between 3 and 6 [13] and is the same as the value reported by Yakabe et al.[3].

From Figs. 2 and 3, η_{Conc} increases as concentrations of H_2 and CO decrease. The increase of η_{Conc} for low reactant concentration is greater than that for high reactant concentration. In other words, the change in η_{Conc} for low reactant concentration is more sensitive to the change of reactant

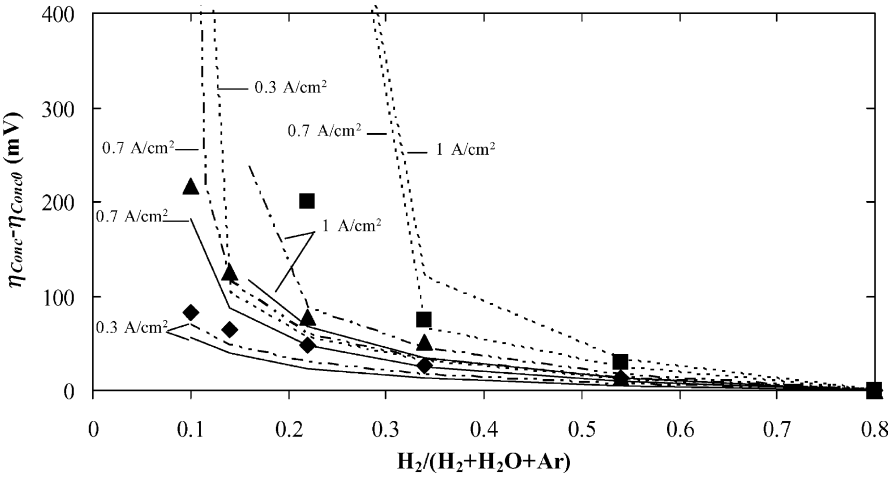

Fig. 2. Comparison between the experimental data and calculated concentration overpotential for the H_2–H_2O–Ar system: symbols represent experimental data, lines simulated ones; (◆) 0.3 A/cm^2, (▲) 0.7 A/cm^2, (■) 1.0 A/cm^2; (- - -) FM, (–·–) DGM, (—) SMM.

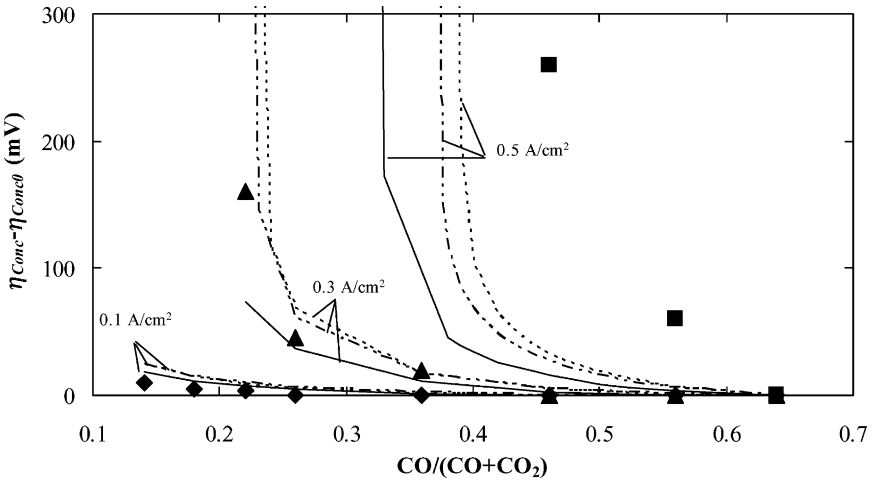

Fig. 3. Comparison of the experimented and calculated concentration overpotential for the CO–CO_2 system: symbols represent experimental data, lines simulated ones; (◆) 0.1 A/cm^2, (▲) 0.3 A/cm^2, (■) 0.5 A/cm^2; (- - -) FM, (–·–) DGM, (—) SMM.

concentration than that for high reactant concentration. When compared among current densities, the increase in current density results in increasing η_{Conc}. The explanation is that η_{Conc} has a greater impact at low fuel concentrations and high operating current densities than at high fuel concentrations and low operating current densities. This is because at high fuel concentration and low operating current densities, the bulk gas contains sufficient reactants to diffuse directly to the anode–electrolyte interface. Consequently, the amount of reactant gas at the anode–electrolyte interface is not much lower than that in the bulk gas. This results in lowering η_{Conc}. On the other hand, at low fuel concentration and high operating current density, the amount of reactant in the bulk gas is not sufficient to attain the desired operating current density. Then, the reactants diffuse slowly to the anode–electrolyte interface. This results in starving reactants at the reaction site (anode–electrolyte interface). It can be noted from experimental and model results that there is a low concentration limit depending on the operating current density below which η_{Conc} increases dramatically. When concentrations of H_2 and CO are near this threshold limit, a small decrease in gas concentration has a tremendous effect on the η_{Conc}. This means that the accuracy in η_{Conc} prediction is crucial for low reactant concentration. Therefore, although the fuel utilization from Yakabe's experiment is less than 5%, the assumption of constant current density is not valid when the fuel concentration is close to its threshold limit. Therefore, the 1-D model is adequate only for fuel concentrations much greater than the threshold limit. However, near the threshold limit a 2-D model is required.

From Fig. 2, it is found that for H_2–H_2O–Ar system, the performance of the DGM in predicting experimented η_{Conc} is as good as that of SMM for high and moderate H_2 concentration. However, its performance is superior to that of the SMM for low H_2 concentration. FM, on the other hand, provides the worst matched results especially at low H_2 concentrations. The reason is that FM uses the concept of equimolar counter diffusion (flux ratio is equal to -1) to derive the overall effective diffusion coefficient as indicated in Eq. (5). This concept is no longer valid when Knudsen diffusion is dominant. In this case, Graham's law, which is derived from the DGM, must be applied to calculate flux ratios. Graham's law states that the flux ratio of diffusion inside porous media relies inversely on the square-root of molecular weight of gas at which the flux ratio is calculated. For the H_2–H_2O–Ar system, $N_{H_2}/N_{H_2O} = -\sqrt{18/2} = -3$ (argon is a stagnant gas), which is very different from -1. Therefore, the assumption of equimolar counter diffusion is not valid. The SMM, on the other hand, can satisfactory assume that equimolar counter diffusion occurs since the porous medium is treated as a stagnant gas film. The Knudsen diffusion term is not taken into account in the SMM. However, this model is not applicable for modeling gas transport phenomena through small pore sizes. Fortunately, the effect of Knudsen diffusion from this model validation is not so critical when compared to molecular diffusion because the pore size is so large that the Knudsen diffusivity ($D_{H_2,k} \approx 28.5\,cm^2/s$) is about four times greater than the binary diffusivity ($D_{H_2–H_2O} \approx 7.1\,cm^2/s$). However, the molecular diffusion depends not only on binary diffusivity but reactant concentration as well. The low molecular diffusion effect is obtained for low reactant concentration. Therefore, the Knudsen diffusion can be crucial to the overall diffusion for low reactant concentration. This explains the reason why the DGM is better than the SMM for predicting η_{Conc} at low H_2 concentrations.

For the CO–CO_2 system, as illustrated in Fig. 3, the performance of FM and the SMM is as good as that of the DGM over the whole range of CO concentration at low current density ($0.1\,A/cm^2$). For moderate current densities ($0.3\,A/cm^2$), both the DGM and FM are somewhat better than that of the SMM especially at low concentration. This can be explained by the fact that the flux ratio of CO to CO_2 is closer to -1 ($N_{CO}/N_{CO_2} = -\sqrt{44/28} = -1.25$). This means that the assumption of equimolar counter diffusion used in FM becomes more valid. In addition, FM takes into account Knudsen diffusion, which is not considered for SMM. In Fig. 3, it is also shown that all models provide bad predictions of the measured data at a current density of $0.50\,A/cm^2$. One possible reason for this is that at high current density, the concentration profile of CO along fuel channel is so different that the assumption of uniform gas distribution is in valid since the diffusion rate of CO is slow.

3.2. Effect of pore size

The influence of pore size is one of the key parameters used to evaluate different mass transport models. This is because an appropriate mass transport model for large pore size may be not suitable for small pore size. Figs. 4 and 5 depict the relationship between pore size and the concentration overpotential (η_{Conc}) for H_2–H_2O and CO–CO_2 systems, respectively. The current densities remain at $1\,A/cm^2$ for H_2–H_2O system and $0.30\,A/cm^2$ for CO–CO_2 system. The typical range of pore size is varied from $1\,\mu m$ (standard size of anode material, [5]) to $2.6\,\mu m$ [3]. This investigation is performed at high, moderate and low reactant concentrations. The mole fractions of reactants are kept at 0.8, 0.4 and 0.25 for high, moderate and low reactant concentrations, respectively. In Figs. 4 and 5, it is obvious that pore size has no effect with using the SMM, which is to be expected since Knudsen diffusion is not taken into consideration. The variable η_{Conc} estimated from both FM and the DGM, in contrast, have the same pattern where it increases as pore size decreases. This means that when pore size is reduced, the Knudsen diffusion becomes predominant due to the decreasing capability of gas to diffuse inside the porous structure. Therefore, the η_{Conc} estimated from both FM and DGM should be equal to or higher than the η_{Conc} obtained from the SMM. However, it is observed that η_{Conc} calculated from the DGM is below η_{Conc} obtained from the SMM for large pore size and high H_2 concentration as shown in Fig. 4(a) in the case of H_2–H_2O system.

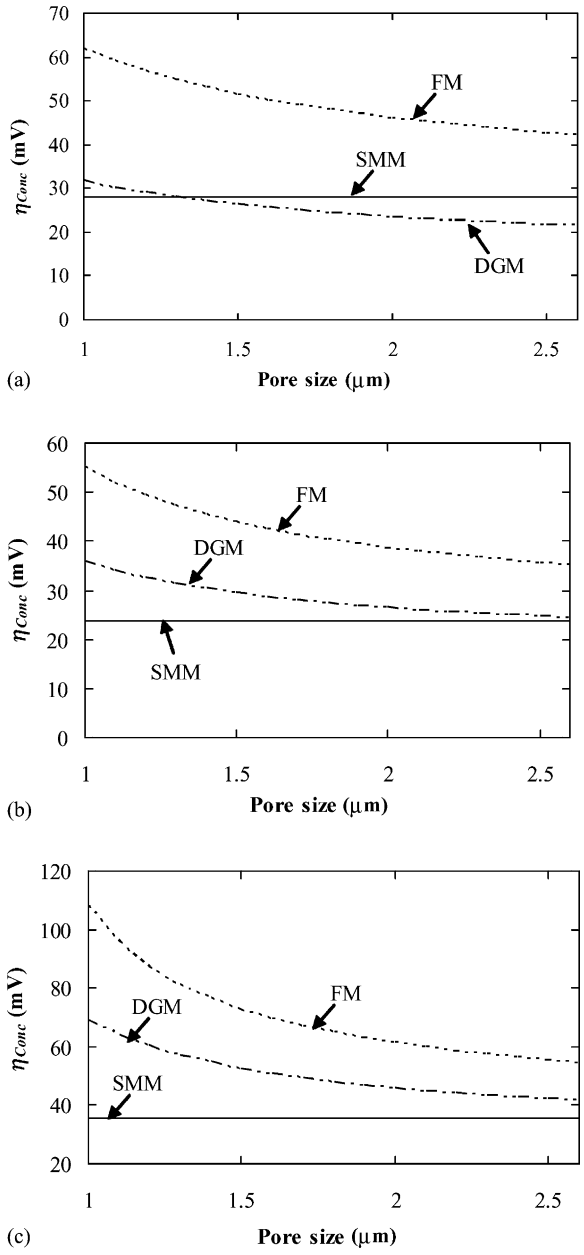

Fig. 4. Relationship between pore size and the concentration overpotential (η_{Conc}) for the H_2–H_2O system at current density = 1 A/cm^2. (a) $H_2/(H_2 + H_2O)$ = 0.80; (b) $H_2/(H_2 + H_2O)$ = 0.40; (c) $H_2/(H_2 + H_2O) = 0.25$.

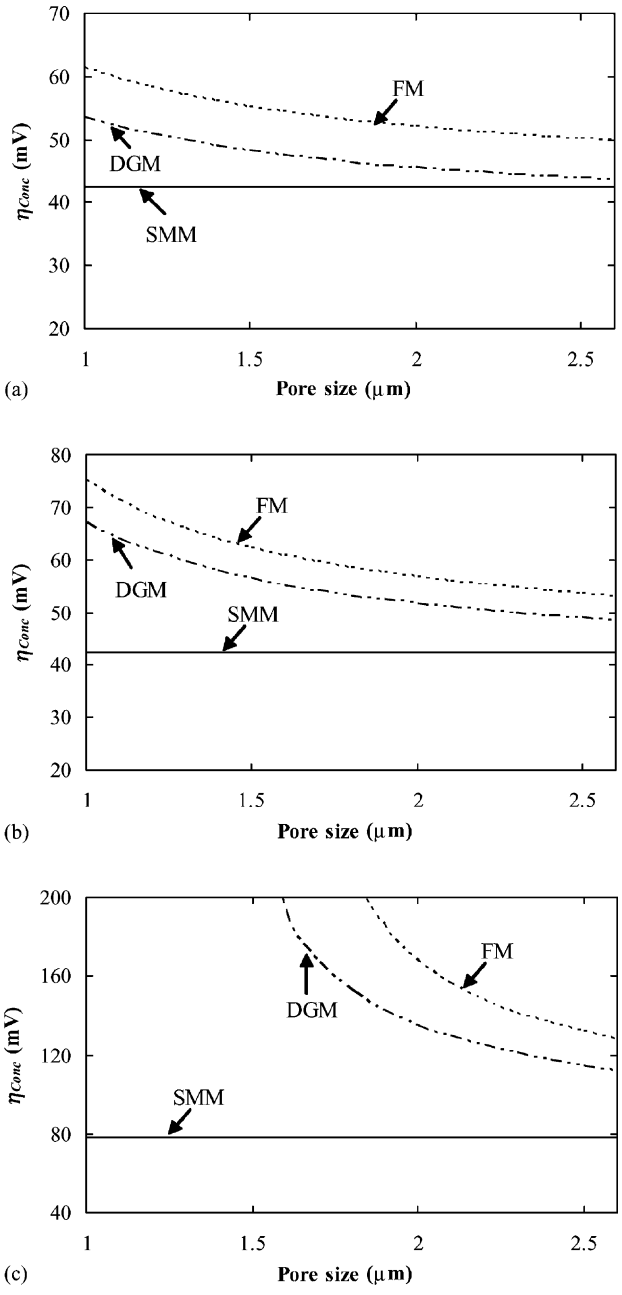

Fig. 5. Relationship between pore size and the concentration overpotential (η_{Conc}) for the CO–CO_2 system at current density = 0.30 A/cm^2. (a) $CO/(CO + CO_2)$ = 0.80; (b) $CO/(CO + CO_2)$ = 0.40; (c) $CO/(CO + CO_2) = 0.25$.

To explain Fig. 4(a) consider the expressions of the flux for both the DGM and the SMM models:

$$N_{H_2} = -\frac{P}{RT}\left(\frac{1}{D^{eff}_{H_2,k}} + \frac{(1-0.67y_{H_2})}{D^{eff}_{H_2-H_2O}}\right)^{-1}\frac{dy_{H_2}}{dz} \quad \text{for the DGM} \tag{29}$$

$$N_{H_2} = -\frac{D^{eff}_{H_2-H_2O}P}{RT}\frac{dy_{H_2}}{dz}, \quad \text{for the SMM} \tag{30}$$

It is observed that there are two parameters that make the DGM different from the SMM; $D^{eff}_{H_2,k}$ and y_{H_2}. For large pore sizes and high concentrations, Knudsen diffusion becomes negligible ($1/D^{eff}_{H_2,k} \to 0$) and Eq. (29) becomes:

$$N_{H_2} = -\frac{D^{eff}_{H_2-H_2O}P}{RT(1-0.67y_{H_2})}\frac{dy_{H_2}}{dz} \quad \text{for the DGM} \tag{31}$$

Comparing Eqs. (30) and (31), it is apparent that the hydrogen molar flux is greater when determined with the DGM

Table 2
Criteria for choosing appropriate mass transport models for CO–CO_2 system

CO concentration (%)	Low current density (0.1 A/cm^2)			High current density (0.3 A/cm^2)		
	Pore size			Pore size		
	Small (<1.5 μm)	Intermediate (1.5–2.0 μm)	Large (>2.0 μm)	Small (<1.5 μm)	Intermediate (1.5–2.0 μm)	Large (>2.0 μm)
Low (25%)	FM	FM	FM	DGM only	DGM only	FM
Intermediate (40%)	FM	FM	FM	FM	FM	FM
High (80%)	DGM only	SMM	SMM	DGM only	SMM	SMM

Remark: DGM is the most accurate model in every case. When FM or SMM is indicated in the table, it means that the results from these models are within 15% of the results obtained from DGM.

than with the SMM. Therefore, for large pore size, η_{Conc} is lower for the DGM than for the SMM.

This behaviour does not occur in the CO–CO_2 system as can be observed in Fig. 5. This is because the flux ratio used in the DGM is almost similar to that used in SMM. Furthermore, the CO molecule is much larger than that of H_2. Therefore, Knudsen diffusion has more impact on the overall diffusion rate even at large pore size. It is also noted that FM always predicts η_{Conc} higher than the DGM. The reason for this is that the flux ratio used in FM is lower than that used in DGM.

From Fig. 4(a) and (b), it is shown that discrepancies between DGM and SMM are smaller than that between the DGM and FM over the entire range of pore size. This means that the SMM is a good approximation of the DGM for high and moderate H_2 concentrations. At low H_2 concentrations, as exhibited in Fig. 4(c), it was found that the SMM is an appropriate model for only moderate and large pore size. This is not an appropriate model for small pore size since the impact of Knudsen diffusion overcomes the molecular diffusion. In this case, it is recommended to use the DGM rather than either FM or the SMM. At high CO concentrations in the CO–CO_2 system, as illustrated in Fig. 5(a), the performance of the SMM in predicting η_{Conc} is superior to that of FM for moderate and large pore sizes. On the other hand, its performance is a somewhat lower than the performance of FM for small pore sizes. However, either FM or the SMM can be applied without significant loss of accuracy. At moderate CO concentrations, as shown in Fig. 5(b), it seems that the difference between the DGM and FM is smaller than that between DGM and SMM over the whole range of pore size. Consequently, it is recommended to use FM in moderate CO concentrations. At low CO concentrations, as depicted in Fig. 5(c), FM is a good approximation of the DGM for large pore size. However, as pore size decreases, both FM and the SMM show large deviations compared to the DGM. Therefore, it is recommended to use the DGM for small and moderate pore sizes.

3.3. Criteria for choosing an appropriate mass transport model

From the performance comparison of the DGM, FM and the SMM for predicting η_{Conc}, it is found that there are three key parameters specifying the criteria for choosing an appropriate mass transport model: current density, reactant concentration and pore size. Although the DGM can predict η_{Conc} accurately, it requires a numerical method to solve. Based on this study, it can be concluded that SMM is a good approximation of the DGM for the H_2–H_2O system except in the case of high current densities, low hydrogen concentrations and small pore sizes where only the DGM is recommended. For the CO–CO_2 system, the criteria for choosing the appropriate mass transport models are summarized in Table 2.

For multicomponent systems such as the H_2–H_2O–CO–CO_2 system, the flux ratios among gas species are so complicated that the equimolar counter diffusion assumption is no longer valid. In this case, it is recommended to use the DGM rather than either FM or the SMM. According to the DGM, as defined in Eq. (14), to derive the flux of each gas species in H_2–H_2O–CO–CO_2 system, it is needed to determine flux ratios of N_{H_2}/N_{H_2O}, N_{CO}/N_{CO_2}, N_{CO}/N_{H_2}, N_{CO}/N_{H_2O}, and N_{CO_2}/N_{H_2}. From Graham's law of diffusion $N_{H_2}/N_{H_2O} = -3$ and $N_{CO}/N_{CO_2} = -1.25$. The electrochemical reactions of H_2 ($H_2 + O^{2-} \rightarrow H_2O + 2e^-$) and CO ($CO + O^{2-} \rightarrow CO_2 + 2e^-$) occur simultaneously. Therefore, the flux ratio of CO to H_2 can be related to the current density produced by CO (J_{CO}) to that generated by H_2 (J_{H_2}), i.e. $N_{CO}/N_{H_2} = J_{CO}/J_{H_2}$. Finally, N_{CO}/N_{H_2O} and N_{CO_2}/N_{H_2} are functions of both J_{CO} and J_{H_2} and are determined to be $-3J_{CO}/J_{H_2}$ and $-0.8J_{CO}/J_{H_2}$, respectively. From this flux ratio calculation, it is demonstrated that the equimolar counter diffusion approach cannot be applied to this system.

4. Conclusions

Mass transport models based on FM, the DGM and the SMM were developed to predict the concentration overpotential inside a SOFC anode. There are a variety of differences between the models. First of all, the SMM does not include the Knudsen diffusion term to account for pore size effect while both FM and the DGM do. Secondly, the equimolar counter diffusion is assumed to determine the flux ratio in both FM and the SMM. By contrast, the flux ratio in the dusty-gas model is calculated from the ratio of the square-root of the gas molecular weight. This is derived

from Graham's law of diffusion. Finally, FM and the SMM can be derived analytically while the DGM requires a numerical solution.

It was found that three parameters define the appropriate mass transport model: current density, reactant concentration and pore size. The DGM is the most suitable model for the H_2–H_2O and CO–CO_2 systems. This is because it takes into account Knudsen diffusion effect as well as Graham's law of diffusion to calculate the flux ratios. However, because of its complexity, this model is only required for conditions of high operating current density, low reactant concentration and small pore size where high accuracy of model prediction is required. otherwise, the SMM is a satisfactorily appropriate model for the H_2–H_2O system while the FM is suitable for the CO–CO_2 system. For the multicomponent system of H_2–H_2O–CO–CO_2; however, the DGM is recommended. This is because the flux ratio calculation is complicated and equimolar counter diffusion cannot be assumed. Furthermore, the Knudsen diffusion effect must be considered.

Acknowledgements

Financial support by the Canadian Program for Energy Research and Development (PERD) and the CANMET CO_2 consortium is gratefully acknowledged.

References

[1] K. Hassmann, Fuel Cells 1 (2001) 78.
[2] J.W. Kim, A.V. Virkar, K.Z. Fung, K. Mehta, S.C. Singhal, J. Electrochem. Soc. 146 (1999) 69.
[3] H. Yakabe, M. Hishinuma, M. Uratani, Y. Matsuzaki, I. Yasuda, J. Power Sources 86 (2000) 423.
[4] S.H. Chan, K.A. Khor, Z.T. Xia, J. Power Sources 93 (2001) 130.
[5] W. Lehnert, J. Meusinger, F. Thom, J. Power Sources 87 (2000) 57.
[6] R.B. Bird, W.E. Stewart, E.N. Lightfoot, Transport Phenomena, Wiley, New York, 1960.
[7] G.F. Froment, K.B. Bischoff, Chemical Reactor Analysis and Design, Wiley, New York, 1990.
[8] R. Krishna, J.A. Wesselingh, Chem. Eng. Sci. 52 (6) (1997) 861.
[9] E.A. Mason, A.P. Malinauskas, Transport in Porous Media: The Dusty Gas Model, Elsevier, New York, 1983.
[10] J.W. Veldsink, R.M.J. Van Damme, G.F. Versteeg, W.P.M. Van Swaaij, Chem. Eng. J. 57 (1995) 115.
[11] J.R. Ferguson, J.M. Fiard, R. Herbin, J. Power Sources 58 (1996) 109.
[12] S.H. Chan, Z.T. Xia, J. Electrochem. Soc. 148 (4) (2001) A388.
[13] M. Iwata, T. Hikosaka, M. Morita, T. Iwanari, K. Ito, K. Onda, Y. Esaki, Y. Sakaki, S. Nagata, Solid State Ionics 132 (2000) 297.
[14] S. Nagata, A. Momma, T. Kato, Y. Kasuga, J. Power Sources 101 (2001) 60.
[15] D. Arnost, P. Schneider, Chem. Eng. J. 57 (1995) 91.
[16] G.J. Borse, Numerical Methods with MATLAB®, PWS Publishing, Boston, 1997.